Analysis of nanoprobe penetration through a lipid bilayer

Fei Liu [a,b,*], Dan Wu [a], Roger D. Kamm [b,c], Ken Chen [a]

[a] State Key Laboratory of Tribology, Department of Mechanical Engineering, Tsinghua University, Beijing, 100084, PR China
[b] Department of Biological Engineering, Massachusetts Institute of Technology, Cambridge, USA
[c] Department Mechanical Engineering, Massachusetts Institute of Technology, Cambridge, USA

ARTICLE INFO

ABSTRACT

With the rapid development of nanotechnology and biotechnology, nanoscale structures are increasingly used in cellular biology. However, the interface between artificial materials and a biological membrane is not well understood, and the harm caused by the interaction is poorly controlled. Here, we utilize the dissipative particle dynamics simulation method to study the interface when a nanoscale probe penetrates the cell membrane, and propose that an appropriate surface architecture can reduce the harm experienced by a cell membrane. The simulation shows that a hydrophilic probe generates a hydrophilic hole around the probe while a hydrophobic probe leads to a 'T-junction' state as some lipid molecules move toward the two ends of the probe. Both types of probe significantly disrupt lipid bilayer organization as reflected by the large variations in free energy associated with penetration of the membrane. Considering the hydrophilic/hydrophobic nature of the lipid bilayer, three other hydrophilic/hydrophobic patterns – band pattern, axial pattern and random pattern – are discussed to reduce the damage to the lipid membrane. Both the free energy analysis and simulation studies show that the axial pattern and the random pattern can both minimize the variations in free energy with correspondingly smaller adverse effects on membrane function. These results suggest that the axial pattern or random pattern nanoprobe generates a mild interaction with the biological membrane, which should be considered when designing nondestructive nanoscale structures.

© 2013 Elsevier B.V. All rights reserved.

1. Introduction

Cell membranes consisting of a lipid bilayer are crucial for living cells providing protection of their interior from the surrounding environment [1]. With rapid advances in biotechnology such as gene injection, in-vitro-fertilization, and drug development, various biological effectors (small molecules, DNAs, RNAs, peptides, and proteins) are required to pass through a cell membrane. One of the promising methods for delivering biological effectors into a cell is to use nanoscale structures (ranging from several to hundreds of nanometers). For example, nanoparticles (<10 nm) [2–6], carbon nanotubes (1 ~ 5 nm) [7–9], and nanowires (~100 nm) [10,11] are considered to be effective methods for introducing multiple types of reagents into cells in high throughput. During delivery, some hydrophilic/hydrophobic molecules adhere to the nanostructures [2,12,13]. However, the lipid bilayer is a thin polar membrane made of two lipid leaflets with hydrophilic phosphate 'heads' on the surface and hydrophobic 'tails' segregated in the core. Because of this 'hydrophilic–hydrophobic–hydrophilic' structure, cell membranes present a formidable barrier to most polar molecules. This means an interface between the artificial materials and the lipid bilayer must be created and surfaces of nanostructures will progressively disrupt the organization of the biomolecules when they come into contact with cell membrane [14–19]. Though, numerous experimental platforms employing nanoscale structures have been constructed to deliver various molecules into different types of cells [2,5,11,20–23]. However, when building such platforms, researchers usually focus on their geometrical size [24], shape [25] or the biological effectors [2] coated on them, and typically pay little attention to the interfaces between the artificial materials and the biological bilayer or the damage experienced by the membrane. In reality, different interfaces will lead to different degrees of bilayer disruption [16,19,25] some causing cell death [22,26]. It is widely accepted that in many cases it is the coated molecules that are interacting with biological system [27–29]. Thus, we propose that an appropriate surface architecture can reduce the harm experienced by a cell membrane and thereby benefit the experimental results. In this paper, we consider a nanoscale probe penetrating the lipid bilayer as an example to study these interactions, with the hope of identifying a surface pattern that is minimally disruptive to cell membranes.

* Corresponding author at: Departments of Mechanical Engineering and Biological Engineering, Massachusetts Institute of Technology (MIT), Room NE47-315, 77 Massachusetts Avenue, Cambridge, MA 02139, USA. Tel.: +1 857 259 8186; fax: +1 617 258 5239.
E-mail address: liufei09@mit.edu (F. Liu).
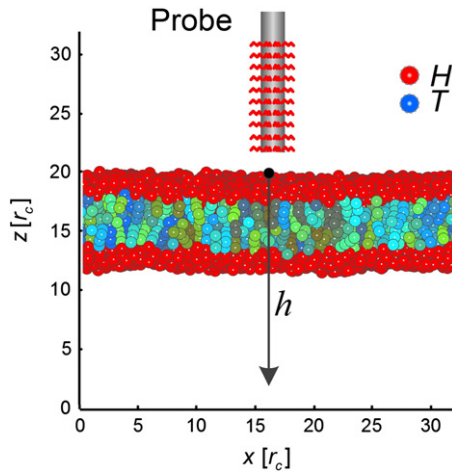
Fig. 1. The simulation model and its initial state, section view with $y = 16r_c$. The tail particles in different chain lipid molecules are colored differently so that they can be distinguished, and for clarity, the water particles are not shown. The probe is $2r_c$ above the membrane at the initial state, thus there is no interaction between the probe and the membrane.

2. Methods

2.1. Dissipative particle dynamics

To analyze the interfaces between the probe and the lipid bilayer, we use dissipative particle dynamics (DPD) simulation, a coarse grained method widely used to study bio-membrane systems [25,30–33]. In

DPD, there are three types of interactive forces: a conservative force, a dissipative force and a random force. The three forces work together to describe the motion of the simulated particles. The conservative force between two particles i and j is

$$F_{ij}^C = a_{ij}\left(1 - r_{ij}/r_c\right)\hat{r}_{ij} \qquad r_{ij} \leq r_c \tag{1}$$

where r_{ij} is the distance between particles i and j, $\hat{r}_{ij}$ is the unit vector connecting particle j to i, and a_{ij} is the conservative force parameter between particles i and j, representing the maximum repulsive force between two types of particles, which differs for different types of particles. The value of a_{ij} for water interacting with another type of particle defines the hydrophilic/hydrophobic character of this type of particle: the larger a_{ij}, the more hydrophobic is the particle. r_c is the cut-off radius; if $r_{ij} > r_c$, the conservative force is zero. r_c is also the length unit used in the simulations [34].

The dissipative force between two particles is linear in terms of their relative momentum and is described as

$$F_{ij}^D = \gamma_{ij}\omega_{ij}^D\left(\hat{r}_{ij} \cdot v_{ij}\right)\hat{r}_{ij} \qquad r_{ij} \leq r_c \tag{2}$$

where γ_{ij} is the dissipative force parameter between particles i and j, and $v_{ij} = v_i - v_j$ is their relative velocity. ω_{ij}^D is the dissipative r-dependent weighting function.

The random force between a particle pair is

$$F_{ij}^R = \sigma_{ij}\omega_{ij}^R\theta_{ij}\frac{1}{\sqrt{\Delta t}}\hat{r}_{ij} \qquad r_{ij} \leq r_c \tag{3}$$

where σ_{ij} is the random force parameter, θ_{ij} is a randomly fluctuating variable with Gaussian statistics and ω_{ij}^R is the random r-dependent weighting function.
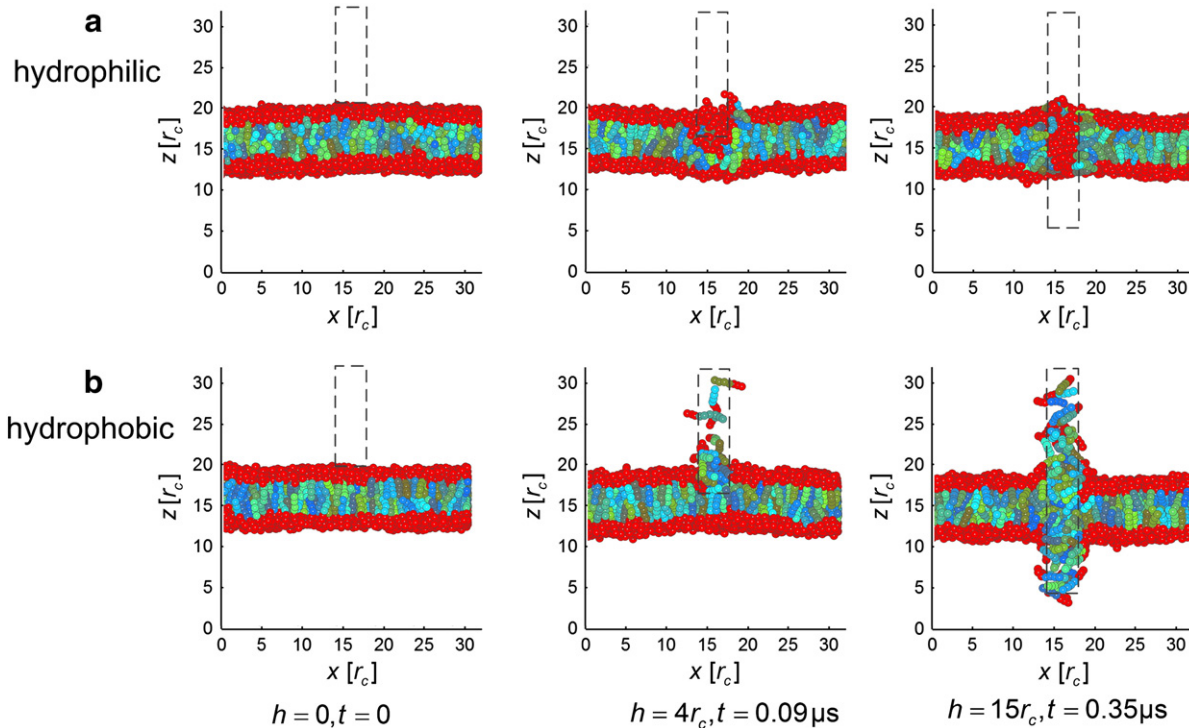
Fig. 2. Morphologies of the lipid bilayer penetrated by hydrophilic and hydrophobic probes, section view with $y = 16r_c$. The dashed rectangles represent the locations of the probe. (a) As the probe descends, for the hydrophilic pattern probe, the head particles of the membrane lipids gather around the probe, and some rotate from vertical to horizontal. (b) For the hydrophobic probe, the tail particles become disordered, and some adhere along the probe, leading to a 'T-junction' state.
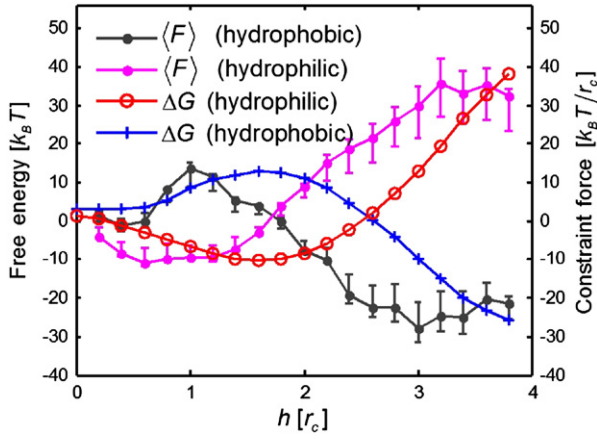
Fig. 3. Free energy and constraint force when hydrophilic and hydrophobic probes are inserted though the membrane. In both cases of hydrophilic or hydrophobic probes, the force and free energy changes rise in magnitude with increasing probe penetration.

Espanol and Warren pointed out that the two weighting functions appearing in Eqs. (2) and (3) follow the relation [35]

$$\omega_{ij}^D = \left(\omega_{ij}^R\right)^2 = \left(1 - r_{ij}/r_c\right)^2 \quad r_{ij} \leq r_c. \tag{4}$$

The dissipative force parameter and random force parameter are related to $\sigma_{ij}^2 = 2\gamma_{ij}k_BT$, where k_B is Boltzmann constant, T is the temperature and k_BT is the unit of energy. The values $\sigma_{ij} = 3$ and $\gamma_{ij} = 4.5$ are used in our model [36].

2.2. Membrane model

In simulation, lipid molecules of the membrane are represented by hydrophobic tail particles (T) and hydrophilic head particles (H). The lipid molecules are surrounded by water particles (W). The thickness of the biological lipid bilayer is ~5–6 nm with ~3 nm hydrophobic core [12,37]. Therefore, the structure of a chain lipid molecule is chosen to be H_3T_4, so as to meet the thickness ratio of the hydrophobic core to the lipid bilayer.
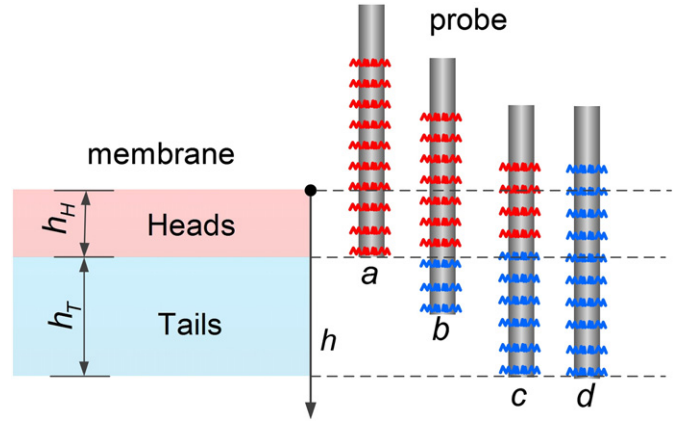
Fig. 5. Penetration of probes with various thicknesses hydrophobic bands. If $h_b = 0$ (hydrophilic pattern, probe a), the minimum free energy happens when $h = h_H$; if $0 < h_b < h_T$ (probe b), the minimum free energy happens when $h = h_H + h_b$; if $h_b = h_T$ (probe c), the minimum free energy is also the lowest free energy in all the different thickness bands when $h = h_H + h_T$. If $h_b > h_T$ (probe d), the minimum free energy happens when $h = h_H + h_T$, but the energy is larger than that of probe c.

In a chain lipid molecule, the H and T particles are linked using Hookean springs with the force

$$\mathbf{F}_{ij}^S = K_S\left(r_{ij} - r_{eq}\right)\hat{\mathbf{r}}_{ij} \tag{5}$$

where particles i and j are adjacent particles in a lipid molecule and r_{eq} is the equilibrium bond length, set to $0.5r_0$. K_S is the spring constant with the value 128 [38].

The hydrocarbon chain stiffness is modelled by the three-body potential acting between adjacent particle triples in a chain

$$U_{\varphi(i-1,i,i+1)} = K_\varphi(1 - \cos(\varphi - \varphi_0)) \tag{6}$$

where the angle φ is defined by the three adjacent particles $i - 1$, i and $i + 1$; φ_0 is the equilibrium angle with preferred value zero; K_φ is the bending constant valued as 20 [38]. Force generated by the three-body potential is

$$\mathbf{F}_{(i-1,i,i+1)}^\varphi = -\nabla U_{\varphi(i-1,i,i+1)}. \tag{7}$$
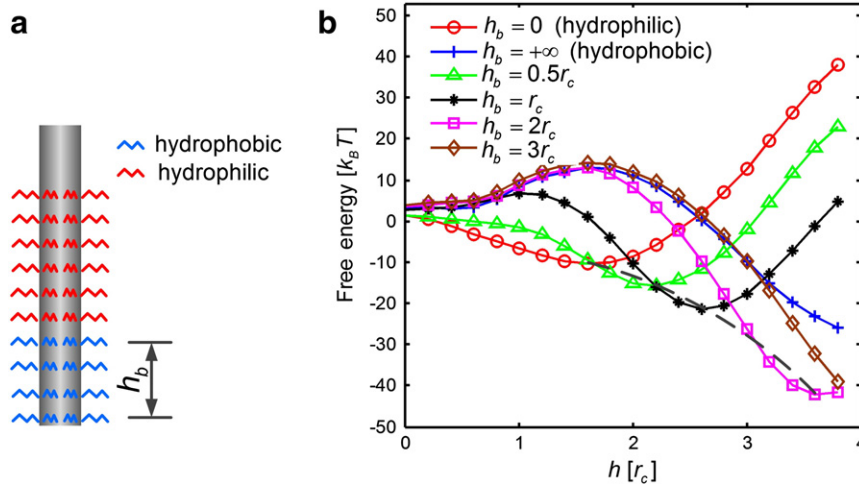
Fig. 4. Band pattern and its free energy analysis. The variations in free energy depend on the thicknesses of hydrophobic bands, and can be reduced to $27.9k_BT$ when $h_b = r_c$. (a) The band pattern probe is functionalized with the hydrophilic and hydrophobic molecules. The hydrophobic molecules are coated at the bottom of the probe as a band of thickness h_b. The rest of the probe is hydrophilic. (b) The free energy for various values of h_b. The dashed line shows the minimum free energy for various probes.

The simulation space is $32 \times 32 \times 32r_c^3$, including 3300 H_3T_4 lipid molecules and 82,000 W particles. The values of conservative force parameters are: $a_{HH} = 25$, $a_{HT} = 50$, $a_{HW} = 35$, $a_{TT} = 25$, $a_{TW} = 75$, and $a_{WW} = 25$ (the subscripts represent the types of particles) [38]. Periodic boundary conditions are applied in all three dimensions to minimize edge effects [39]. The particles are assembled into a planar bilayer in a tension-free state at room temperature. The membrane model is depicted in Fig. 1 with, the H particles on the surface of the membrane, and the T particles in the middle, indicating a classical lipid bilayer structure (the W particles are not drawn for clarity). The thickness of the membrane is ~ $7.5r_c$ and the hydrophobic core is ~ $4.5r_c$ or 60% of the thickness of the membrane. Considering the physical thickness of a membrane (5–6 nm) and the diffusion coefficient of lipid bilayer (5 μm²/s), the length unit in simulation model $r_c \approx 0.7$ nm and the time unit $\tau \approx 0.46$ ns [34].

To simulate the process of a probe penetrating the lipid membrane, a cylindrical probe model is introduced into the DPD membrane model. The cylindrical probe is composed of 1130 probe particles (P), each with a diameter $4r_c$ (~3 nm) and height $30r_c$. To determine the movement of the probe, probe position h is measured relative to a coordinate system centered at ($16r_c$, $16r_c$, $20r_c$), just at the upper surface of the membrane, and in the initial state, the bottom of the probe is located $2r_c$ above the membrane. Under these initial conditions there is no interaction between the probe and the membrane.

In DPD, the conservative force parameter (a_{ij}) reflects the repulsive force between two types of particles. Smaller value of the conservative force parameter means 'attraction'. The value of a_{ij} for water particle interacting with another type of particle defines the hydrophilic/hydrophobic character of this type of particle: the larger a_{ij}, the more hydrophobic is the particle [34,38]. Thus, for a hydrophilic probe (all the coated molecules are hydrophilic), the values of conservative force parameters are $a_{PW} = 35$, $a_{PT} = 75$, and $a_{PH} = 15$, while for a hydrophobic probe, these values change to $a_{PW} = 50$, $a_{PT} = 15$, and $a_{PH} = 75$. The bilayer is relaxed for 1.2 μs with the probe fixed at first. Then, the probe is displaced downwards at a constant velocity of $0.02r_c/\tau$, with the physical value ~0.03 nm/ns. We tested velocities ranging from $0.05r_c/\tau$ to $0.001r_c/\tau$ for a hydrophilic probe, and the results were found to be similar (results not shown). Although a lower velocity generally leads to a more precise calculation, it also requires additional computing time. This chosen velocity is acceptable from the perspective of computational time and is of comparable magnitude to the average velocity of a nanoparticle penetrating the membrane under a driving force [25,40]. In our model, the nanoprobe is forced to move downwards at a specific velocity. Therefore, under the conditions we impose, the nanoprobe will always penetrate through the membrane even if the velocity is reduced
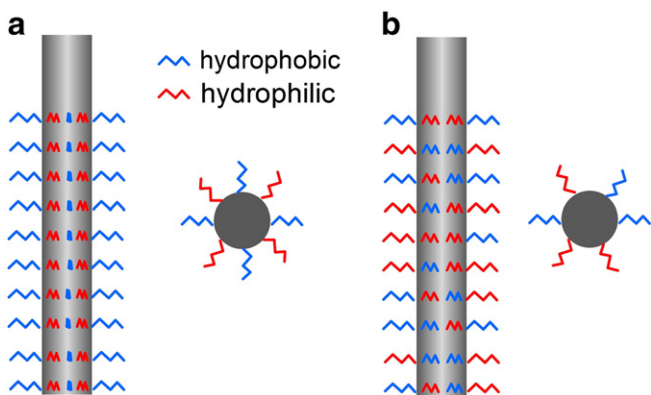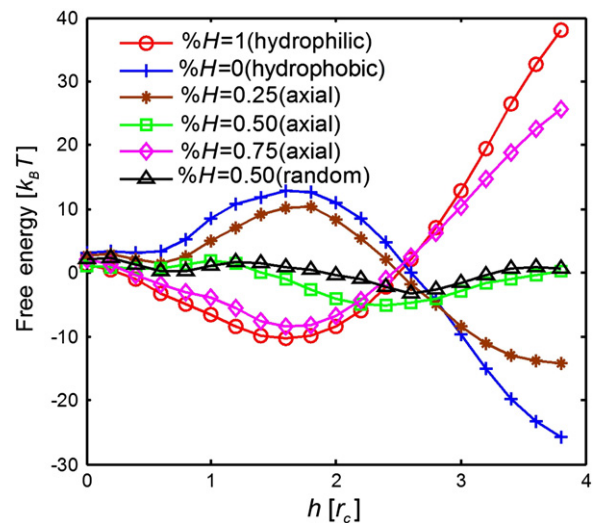

Fig. 7. The free energy of axial pattern and random pattern probes penetrating a membrane. For the axial pattern, the probe circumference is equally divided into 24 parts, and 6, 12, or 18 parts are H particles (%H = 0.25, 0.5, 0.75). The variations in free energy are related to the % H, and are smallest when %H = 0.5 for both axial and random patterns.

further. If the nanoprobe is driven instead by a specific force, it could wind up stalling in the membrane [25]. During penetration, the probe particles interact with and influence the positions and velocities of the $H/T/W$ particles. However, the velocity and the position of the probe are specified, thus the interaction forces from $H/T/W$ particles to the probe are ignored.

3. Results and discussion

The membrane's morphologies during the process of penetration by hydrophilic and hydrophobic probes, respectively, are shown in Fig. 2. In Fig. 2a, the hydrophilic heads of the lipid bilayer are attracted to contact with the probe while the hydrophobic heads are repelled, leading to a hole with the hydrophilic edge around the probe. In the hydrophobic case (Fig. 2b) the lipid bilayer is split, and the tail particles are attracted to adhere along the probe, whereas the heads are pushed toward the water. Some of the tail particles move toward the two ends of the probe, generating a 'T-junction' scenario.

Due to the interaction between the probe and membrane, the hydrophilic and hydrophobic patterns lead to a major disruption of the lipid organization (Fig. 2). During penetration, work done by the attractive or repulsive forces changes the energy of the system. If the variation in energy is too strong, the lipid molecules may be disordered. Therefore, a nondestructive pattern should avoid such interactions. Considering the hydrophilic/hydrophobic composition of the lipid bilayer, it is possible to change the probe's hydrophilic/hydrophobic pattern in order to find an appropriate probe design to minimize these destructive effects.

For quantitative analysis, the method of constrained particles is applied to calculate the free energy, ΔG, when a probe penetrates the membrane, Eq. (8) [41,42]. During calculation, the probe is placed at a chosen z-depth in the membrane. The force acting on the probe at each time step is obtained as the constraint force at that z-depth. For each of the z-depths, nine different x and y regions of the membrane are sampled, and for each region, the simulation time is 3000 time steps. By measuring the average z-force needed to keep the constraint, and integrating across the membrane, the potential of mean force or the free energy is constructed.

Fig. 6. The axial pattern and random pattern probes. (a) Axial pattern: the hydrophilic and hydrophobic molecules are coated in lines parallel to the axis of the cylinder (left), and it is symmetrical as seen from top view (right). (b) Random pattern: the molecules are located at random positions.

$$\Delta G = - \int_0^h \langle F \rangle \, dh \quad 0 \le h \le 3.8r_c \qquad (8)$$

Here, $\langle F \rangle$ indicates average constraint force over the simulation time. Because of the symmetry of the membrane, h is analyzed from 0 to $3.8r_c$ representing the upper layer of the bilayer membrane. Fig. 3 shows the free energy and constraint force of the hydrophilic pattern and hydrophobic pattern probes shown in Fig. 2. For the hydrophilic probe, at the beginning of the penetration, the free energy is less than zero indicating that the force is attractive between the probe and the hydrophilic heads of membrane. When the hydrophilic probe enters into the hydrophobic core of the lipid bilayer, the free energy rises, and at a certain point the free energy becomes >0 suggesting that the membrane repels the penetration of the probe. It is opposite if the probe is hydrophobic, with the interactive force changing from repulsive to attractive.

The variations in free energy for the hydrophilic and hydrophobic patterns are $48.3k_BT$ and $38.7k_BT$, respectively (Fig. 3). These results suggest that a less destructive penetration might be achieved using probes having various patterns of both hydrophilic and hydrophobic regions. Based on this idea, the band pattern probe [12,19] is designed with a hydrophobic band at its bottom with the thickness h_b (Fig. 4a). Fig. 4b presents the free energy for various values of h_b.

It shows that the free energy changes owning to the different thickness bands. However, the minimum variation in free energy happens when $h_b = r_c$ with the value $27.9k_BT$, which suggests that the changing of thickness of the hydrophobic bands does not reduce the variation in free energy too much. To support this idea, we provide a further explanation by calculating the minimum free energy of various bands. Fig. 5 shows the penetration of probes with various thickness bands. If the probe is hydrophilic, the minimum free energy happens when the probe is at the interface of lipid's heads and tails (probe a). However, if there is a hydrophobic band at the bottom of the probe, the minimum free energy happens when all the bands immerge into the lipid tails while the hydrophilic region of the
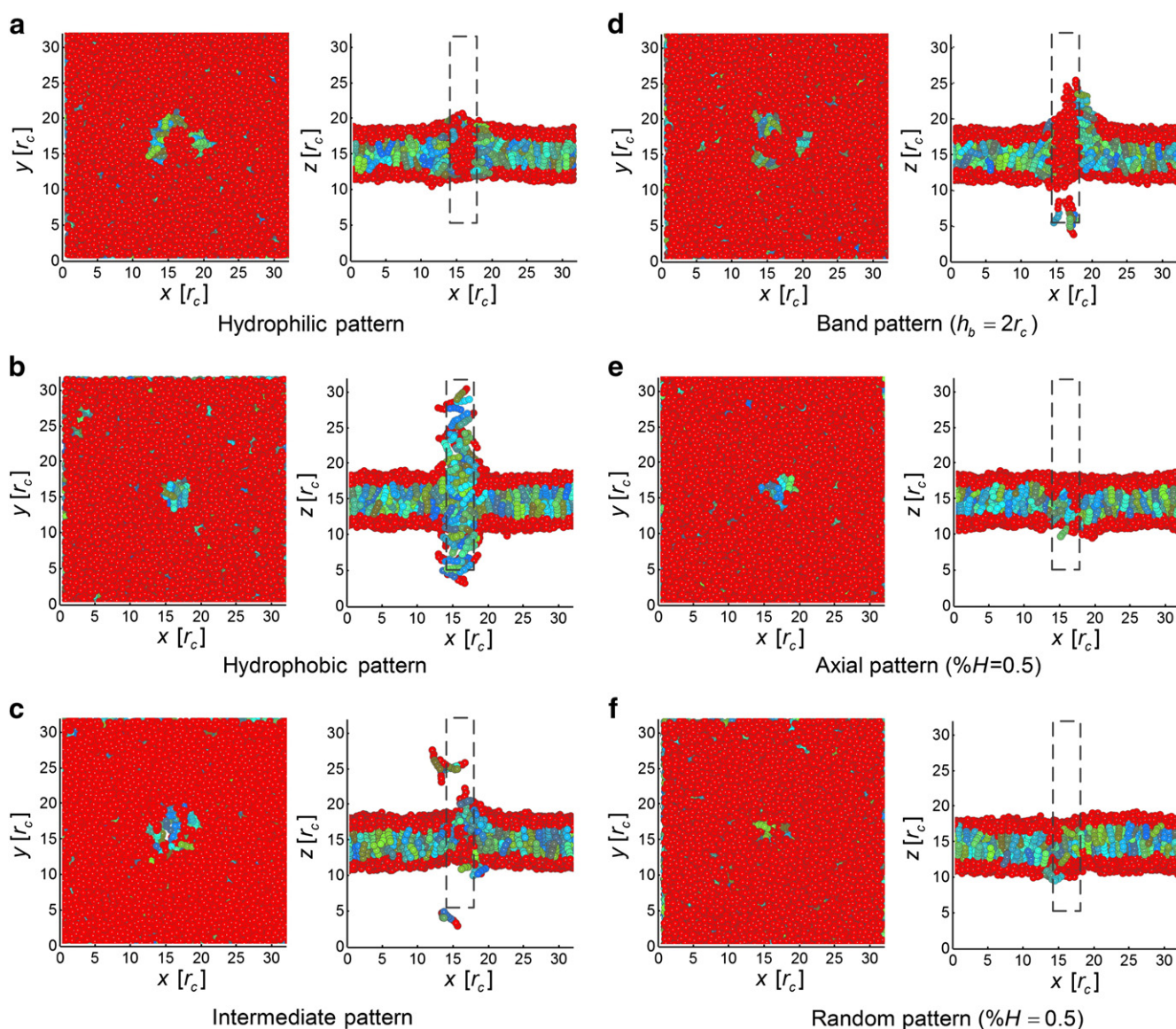
Fig. 8. Morphologies of lipid membranes penetrated by five probes with different patterns when $h = 15r_c$, $t = 0.35\mu s$; top view and section views with $y = 16r_c$. (a) Hydrophilic pattern. The hydrophilic heads gather around the probe. (b) Hydrophobic pattern. Some molecules move toward the ends of the probe leading to a 'T-junction'. (c) Intermediate pattern. There is a mixture of hydrophilic heads and hydrophobic tails around the probe. (d) Band pattern with $2r_c$ band thickness. The movement of lipid molecules is a combination of that observed with hydrophilic and hydrophobic patterns. (e) Axial pattern with $\%H = 0.5$; (f) random pattern with $\%H = 0.5$. Both axial pattern and random pattern help maintain the bilayer organization of the membrane.

probe is fully contact with the lipid heads (probe b, c). By comparing the two states, it is concluded that the probe with band has a lower minimum free energy due to the attractive force between the hydrophobic band and lipid tails. The dash line in Fig. 4b shows the trend of the minimum free energy of various thickness bands. Therefore, if there is a hydrophobic band, the minimum free energy of the band pattern will be lower than that of hydrophilic pattern which is $-10.3k_BT$ (Fig. 3). Fig. 5 also indicates that the lowest free energy for all the different thickness bands takes place when $h = h_H + h_T$ with the band thickness $h_b = h_T$, where h_H and h_T are the thicknesses of the head region and tail region, respectively (probe c). These results correspond to the positions of turning points in Figs. 3 and 4.

We next consider a different probe pattern (Fig. 6a) in which the hydrophobic and hydrophilic molecules are coated in lines parallel to the axis of the cylinder. The percentage of H particles in probe particles, $\%H$, is used to characterize the pattern. Viewed along the axis, the coated hydrophobic and hydrophilic molecules are arranged with axial symmetry and the probe circumference is finely divided in order to avoid unbalanced forces in the x and y directions. We also consider cases in which the hydrophobic and hydrophilic molecules are located at random (Fig. 6b).

The penetration of the probe will change the interaction from head–head/tail–tail to probe–head/probe–tail. The larger difference between the probe-head interaction and head–head interaction (indicated by $|a_{PH} - a_{HH}|$) or between the probe–tail and tail–tail interaction (indicated by $|a_{PT} - a_{TT}|$), the greater is the disruption of the membrane. The variations in free energy of penetration with the axial and random patterns (Fig. 7) depend on the percentage of H particles ($\%H$). When $\%H = 0.5$, both patterns can reduce the variation to relatively small values, $6.0k_BT$ and $4.9k_BT$, respectively, which suggests that either of the two patterns can serve as nondestructive structures. A value for $\%H \approx 0.5$ appears to be nearly optimal in terms of minimizing the variation in free energy (Fig. 7). This percentage depends on the probe's degree of hydrophobicity, represented by the conservative force parameters in DPD. Because the absolute values of force and free energy for the hydrophilic and hydrophobic patterns are similar (Fig. 3), when $\%H \approx 0.5$, the sum of free energies due to the hydrophobic and hydrophilic regions roughly cancels each other giving rise to the relatively small variation during penetration. Further analysis shows that for a strongly hydrophobic and a lightly hydrophilic probe, with the conservative force parameters $a_{PW} = 35$, $a_{PT} = 50$, $a_{PH} = 20$ (hydrophilic region, representing light hydrophilic), $a_{PW} = 50$, $a_{PT} = 10$, and $a_{PH} = 100$ (hydrophobic region, representing strong hydrophobic), $\%H = 0.25$ is a more appropriate percentage causing the minimal variation in energy. Moreover, if the probe is intermediate (non-hydrophilic and non-hydrophobic) with conservative force parameters $a_{PW} = 50$, $a_{PT} = 50$, and $a_{PH} = 50$, it repels the hydrophilic heads and hydrophobic tails equally. Therefore, there would be a mixture of heads and tails.

To verify these findings from energy analysis, four additional patterns – intermediate pattern ($a_{PW} = 50$, $a_{PT} = 50$, $a_{PH} = 50$), band pattern ($h_b = 2r_c$), axial pattern ($\%H = 0.5$), and random pattern ($\%H = 0.5$) – are simulated, producing the membrane morphologies shown in Fig. 8. After penetration, some lipid molecules rotate horizontally in order to come in contact with the hydrophilic probe (Fig. 8a); the hydrophobic probe induces that some of the lipid molecules emerge from the membrane and adhere to the hydrophobic probe (Fig. 8b). The intermediate pattern leads to a mixture of heads and tails around the probe due to the equal interactive force (Fig. 8c). The movement of lipid molecules in Fig. 8d seems a combination of that in Fig. 8a and b, with some of the lipid molecules leaving the membrane by rotating from vertical to horizontal. In contrast, most of the lipid molecules maintain their normal orientations along with z axis, suggesting that there is little force generated during penetration (Fig. 8e and 8f). These simulation results support the conclusions of the free energy analysis.

4. Conclusions

In conclusion, our analysis of the interaction between nanoscale probes penetrating a biological membrane shows that different patterns of hydrophilic/hydrophobic coatings on the probe surface will create different interfaces between lipid bilayers. If the probe is hydrophilic, the interface is a hydrophilic hole by the probe, while it generates a 'T-junction' scenario when the probe has a hydrophobic surface. In order to reduce the damage caused to the membrane, we use the free energy to describe disruption of the lipid membrane quantitatively. The band pattern, axial pattern, and the random pattern are considered for their potential to minimize variations in energy. Both the free energy analysis and simulation results show that the axial and random patterns cause less disruption to the lipid bilayer organization. Therefore, when using nanoprobes to penetrate a lipid membrane, the axial pattern or random pattern should be considered as a means of reducing membrane disruption.

References

[1] P.L. Yeagle, Cholesterol and the cell membrane, Biochim. Biophys. Acta 822 (1985) 267–287.
[2] A. Verma, O. Uzun, Y. Hu, Y. Hu, H.S. Han, N. Watson, S. Chen, D.J. Irvine, F. Stellacci, Surface-structure-regulated cell-membrane penetration by monolayer-protected nanoparticles, Nat. Mater. 7 (2008) 588–595.
[3] X.H.N. Xu, W.J. Brownlow, S.V. Kyriacou, Q. Wan, J.J. Viola, Real-time probing of membrane transport in living microbial cells using single nanoparticle optics and living cell imaging, Biochemistry 43 (2004) 10400–10413.
[4] A. Pramanik, D. Laha, D. Bhattacharya, P. Pramanik, P. Karmakar, A novel study of antibacterial activity of copper iodide nanoparticle mediated by DNA and membrane damage, Colloids Surf. B 96 (2012) 50–55.
[5] K.T. Thurn, E.M.B. Brown, A. Wu, S. Vogt, B. Lai, J. Maser, T. Paunesku, G.E. Woloschak, Nanoparticles for applications in cellular imaging, Nanoscale Res. Lett. 2 (2007) 430–441.
[6] R. Vácha, F.J. Martinez-Veracoechea, D. Frenkel, Receptor-mediated endocytosis of nanoparticles of various shapes, Nano Lett. 11 (2011) 5391–5395.
[7] W. Yang, P. Thordarson, J.J. Gooding, S.P. Ringer, F. Braet, Carbon nanotubes for biological and biomedical applications, Nanotechnology 18 (2007) 412001.
[8] M.G. Schrlau, H.H. Bau, Carbon-based nanoprobes for cell biology, Microfluid. Nanofluid. 7 (2009) 439–450.
[9] N.W.S. Kam, T.C. Jessop, P.A. Wender, H. Dai, Nanotube molecular transporters: internalization of carbon nanotube-protein conjugates into mammalian cells, J. Am. Chem. Soc. 126 (2004) 6850–6851.
[10] A.K. Shalek, J.T. Robinson, E.S. Karp, J.S. Lee, D.R. Ahn, M.H. Yoon, A. Sutton, M. Jorgolli, R.S. Gertner, T.S. Gujral, Vertical silicon nanowires as a universal platform for delivering biomolecules into living cells, Proc. Natl. Acad. Sci. U. S. A. 107 (2010) 1870–1875.
[11] W. Kim, J.K. Ng, M.E. Kunitake, B.R. Conklin, P. Yang, Interfacing silicon nanowires with mammalian cells, J. Am. Chem. Soc. 129 (2007) 7228–7229.
[12] B.D. Almquist, N.A. Melosh, Molecular structure influences the stability of membrane penetrating biointerfaces, Nano Lett. 11 (2011) 2066–2070.
[13] R.C. Van Lehn, A. Alexander-Katz, Penetration of lipid bilayers by nanoparticles with environmentally-responsive surfaces: simulations and theory, Soft Matter 7 (2011) 11392–11404.
[14] V.K. Gangupomu, F.M. Capaldi, Interactions of carbon nanotube with lipid bilayer membranes, J. Nanomater. 2011 (2011) 1–6, http://dx.doi.org/10.1155/2011/830436, (Article ID 830436).
[15] H. Ding, W. Tian, Y. Ma, Designing nanoparticle translocation through membranes by computer simulations, ACS Nano 6 (2012) 1230–1238.
[16] A.A. Skandani, R. Zeineldin, M. Al-Haik, Effect of chirality and length on the penetrability of single-walled carbon nanotubes into lipid bilayer cell membranes, Langmuir 28 (2012) 7872–7879.
[17] C. Chipot, M. Tarek, Interaction of a peptide nanotube with a water–membrane interface, Phys. Biol. 3 (2006) S20.
[18] E.J. Wallace, M.S.P. Sansom, Carbon nanotube self-assembly with lipids and detergent: a molecular dynamics study, Nanotechnology 20 (2008) 045101.
[19] B.D. Almquist, P. Verma, W. Cai, N.A. Melosh, Nanoscale patterning controls inorganic–membrane interface structure, Nanoscale 3 (2010) 391–400.
[20] A. Hultgren, M. Tanase, C. Chen, G. Meyer, D. Reich, Cell manipulation using magnetic nanowires, J. Appl. Phys. 93 (2003) 7554–7556.

[21] W. Jiang, B.Y.S. Kim, J.T. Rutka, W.C.W. Chan, Nanoparticle-mediated cellular response is size-dependent, Nat. Nanotechnol. 3 (2008) 145–150.

[22] A.E. Nel, L. Mädler, D. Velegol, T. Xia, E.M.V. Hoek, P. Somasundaran, F. Klaessig, V. Castranova, M. Thompson, Understanding biophysicochemical interactions at the nano-bio interface, Nat. Mater. 8 (2009) 543–557.

[23] X. Chen, A. Kis, A. Zettl, C.R. Bertozzi, A cell nanoinjector based on carbon nanotubes, Proc. Natl. Acad. Sci. U. S. A. 104 (2007) 8218–8222.

[24] S. Zhang, A. Nelson, P.A. Beales, Freezing or wrapping: the role of particle size in the mechanism of nanoparticle–biomembrane interaction, Langmuir 28 (2012) 12831–12837.

[25] K. Yang, Y.Q. Ma, Computer simulation of the translocation of nanoparticles with different shapes across a lipid bilayer, Nat. Nanotechnol. 5 (2010) 579–583.

[26] P.R. Leroueil, S. Hong, A. Mecke, J.R. Baker Jr., B.G. Orr, M.M. Banaszak Holl, Nanoparticle interaction with biological membranes: does nanotechnology present a Janus face? Acc. Chem. Res. 40 (2007) 335–342.

[27] M.P. Monopoli, C. Åberg, A. Salvati, K.A. Dawson, Biomolecular coronas provide the biological identity of nanosized materials, Nat. Nanotechnol. 7 (2012) 779–786.

[28] T. Cedervall, I. Lynch, S. Lindman, T. Berggård, E. Thulin, H. Nilsson, K.A. Dawson, S. Linse, Understanding the nanoparticle–protein corona using methods to quantify exchange rates and affinities of proteins for nanoparticles, Proc. Natl. Acad. Sci. U. S. A. 104 (2007) 2050–2055.

[29] D. Walczyk, F.B. Bombelli, M.P. Monopoli, I. Lynch, K.A. Dawson, What the cell "sees" in bionanoscience, J. Am. Chem. Soc. 132 (2010) 5761–5768.

[30] R. Groot, K. Rabone, Mesoscopic simulation of cell membrane damage, morphology change and rupture by nonionic surfactants, Biophys. J. 81 (2001) 725–736.

[31] R. Goetz, R. Lipowsky, Computer simulations of bilayer membranes: self-assembly and interfacial tension, J. Chem. Phys. 108 (1998) 7397–7409.

[32] S. Ramachandran, P. Kumar, M. Laradji, Lipid flip–flop driven mechanical and morphological changes in model membranes, J. Chem. Phys. 129 (2008) 125104.

[33] A. Alexeev, W.E. Uspal, A.C. Balazs, Harnessing Janus nanoparticles to create controllable pores in membranes, ACS Nano 2 (2008) 1117–1122.

[34] G. Illya, R. Lipowsky, J. Shillcock, Effect of chain length and asymmetry on material properties of bilayer membranes, J. Chem. Phys. 122 (2005) 244901.

[35] P. Espanol, P. Warren, Statistical mechanics of dissipative particle dynamics, Europhys. Lett. 30 (1995) 191.

[36] V. Ortiz, S.O. Nielsen, D.E. Discher, M.L. Klein, R. Lipowsky, J. Shillcock, Dissipative particle dynamics simulations of polymersomes, J. Phys. Chem. B 109 (2005) 17708–17714.

[37] J.F. Nagle, S. Tristram-Nagle, Structure of lipid bilayers, Biochim. Biophys. Acta 1469 (2000) 159–195.

[38] L. Gao, J. Shillcock, R. Lipowsky, Improved dissipative particle dynamics simulations of lipid bilayers, J. Chem. Phys. 126 (2007) 015101.

[39] R.D. Groot, P.B. Warren, Dissipative particle dynamics: bridging the gap between atomistic and mesoscopic simulation, J. Chem. Phys. 107 (1997) 4423.

[40] Y. Li, T. Yue, K. Yang, X. Zhang, Molecular modeling of the relationship between nanoparticle shape anisotropy and endocytosis kinetics, Biomaterials 33 (2012) 4965–4973.

[41] D. Bemporad, C. Luttmann, J. Essex, Computer simulation of small molecule permeation across a lipid bilayer: dependence on bilayer properties and solute volume, size, and cross-sectional area, Biophys. J. 87 (2004) 1–13.

[42] S.J. Marrink, H.J.C. Berendsen, Permeation process of small molecules across lipid membranes studied by molecular dynamics simulations, J. Phys. Chem. 100 (1996) 16729–16738.